HHS Public Access

Author manuscript

Med Image Comput Comput Assist Interv. Author manuscript; available in PMC 2019 December 04.

Published in final edited form as:

Med Image Comput Comput Assist Interv. 2018 September ; 11070: 853–861. doi: 10.1007/978-3-030-00928-1_96.

Hierarchical Spherical Deformation for Shape Correspondence

Ilwoo Lyu[1], **Martin A. Styner**[2], **Bennett A. Landman**[1]

[1]Electrical Engineering and Computer Science, Vanderbilt University, TN, USA

[2]Psychiatry, The University of North Carolina at Chapel Hill, NC, USA

Abstract

We present novel spherical deformation for a landmark-free shape correspondence in a group-wise manner. In this work, we aim at both addressing template selection bias and minimizing registration distortion in a single framework. The proposed spherical deformation yields a non-rigid deformation field without referring to any particular spherical coordinate system. Specifically, we extend a rigid rotation represented by well-known Euler angles to general non-rigid local deformation via spatial-varying Euler angles. The proposed method employs spherical harmonics interpolation of the local displacements to simultaneously solve rigid and non-rigid local deformation during the optimization. This consequently leads to a continuous, smooth, and hierarchical representation of the deformation field that minimizes registration distortion. In addition, the proposed method is group-wise registration that requires no specific template to establish a shape correspondence. In the experiments, we show an improved shape correspondence with high accuracy in cortical surface parcellation as well as significantly low registration distortion in surface area and edge length compared to the existing registration methods while achieving fast registration in 3 mins per subject.

Keywords

shape correspondence; spherical harmonics interpolation; spherical mapping; surface registration

1 Introduction

Understanding of morphology in medical imaging is a fundamental step for statistical analyses of cortical structures such as anatomy, pathology, and physiology. This typically requires well establishment of a shape correspondence, which might otherwise result in an unacceptable analysis. For example, studies of brain degeneration such as Alzheimer's disease rely on a proper shape correspondence of cortical structures for a valid comparison of local cortical measurements. However, most cortical structures are highly variable in general; therefore, it is quite challenging to define a formal consensus in the existence of such variability.

Spherical deformation has been widely used for surface registration [3,7,4,6]. Several template-based methods have been proposed without referring to a specific spherical

ilwoo.lyu@vanderbilt.edu.

coordinate system [3,7,6]. In [7], spherical displacements are represented as local geodesics in the local tangent space but only capture local deformation after applying an initial rigid rotation. [6] discretized the local spherical deformation using fixed sampling points. The degree of freedom of deformation is limited to the number of the points. Alternatively [4] proposed a template-free method via spherical harmonics interpolation of local angular displacements. However, the quality of their deformation depends on a spherical coordinate system due to linear interpolation of non-linear polar angles. This yields an inconsistent deformation field having instability around the poles.

A desirable property to surface registration is to reduce registration distortion while maximizing similarity metrics. Even with high registration accuracy, registration distortion could still exist due to template bias or missing anatomy, which potentially affects secondary statistical shape analyses. For instance, [6] showed that a shape correspondence with reduced registration distortion improves statistical sensitivity in secondary analyses. Such registration distortion can be reduced with deformation regularization [3,7,6] or without employing a template in an unbiased fashion [4]. In addition to the smoothness of deformation fields, an optimal rigid alignment can minimally allow non-rigid local deformation. However, most surface registration methods typically use either a specific template or an initial rigid alignment once before non-rigid deformation.

In this paper, we propose novel spherical deformation that minimizes registration distortion. The proposed method harmonizes rigid and non-rigid deformation in a single framework. Specifically, it achieves global rigid alignment during the optimization while simultaneously allowing spatial-varying local deformation as a function of each spherical location. Moreover, the proposed method is group-wise registration without referring to a specific template. Our method is inspired by spherical harmonics interpolation of deformation fields [4]. In contrast to their spherical deformation relying heavily on initial optimal pole selection, however, the proposed method does not refer to any particular spherical coordinate system. This thus yields a well-established shape correspondence with lower registration distortion in 3 mins per subject than the existing methods [3,7].

2 Methods

2.1 Problem Definition

We consider a set of N cortical surfaces with their initial spherical mappings. For the ith subject, the goal is to estimate a continuous spherical deformation field $M^i: \mathbb{S}^2 \to \mathbb{S}^2$ such that

$$M^1\left(\mathbf{x}^1\right) = M^2\left(\mathbf{x}^2\right) = \cdots = M^N\left(\mathbf{x}^N\right), \tag{1}$$

where $\mathbf{x}^i \in \mathbb{S}^2$ is the corresponding location of the ith subject. In principle, M provides displacements carrying any spherical locations to their corresponding ones. A desirable deformation field is smooth and continuous. Here, a key component is thus to represent spherical displacements of the corresponding locations appropriately that meet such a

demand. In the following sections, we first describe the proposed displacement encoding scheme represented by a rigid rotation and then extend the idea to non-rigid deformation.

2.2 Displacement Encoding

We consider a displacement on the unit sphere. We seek a consistent displacement encoding scheme free from a non-linear spherical polar coordinate system. Here, an Euler rotation can efficiently encode such a displacement by the composition of two independent rotations: rotation of an Euler axis followed by rotation about the Euler axis. Figure 1 shows a schematic illustration of the proposed encoding.

Euler axis.—Any reference Euler axis can sufficiently implement a target rigid rotation. Euler's rotation theorem implies that intermediate rotations (of and about an Euler axis) vary depending on a reference Euler axis but their composite rotation is equivalent to any target rotation independent of a reference Euler axis. Therefore we choose an arbitrary Euler axis (e.g., north pole) denoted by $\mathbf{z} \in \mathbb{S}^2$.

Rotation of Euler axis.—We consider $\mathbf{z}$ is rotated to be at $\hat{\mathbf{z}} \in \mathbb{S}^2$. The location of $\hat{\mathbf{z}}$ is given as a function of two polar angles $(\alpha, \beta) \in [0, \pi] \times [-\pi, \pi]$.

$$\hat{\mathbf{z}}(\alpha, \beta) = \left[\sin(\alpha_{\mathbf{z}} + \alpha)\cos(\beta_{\mathbf{z}} + \beta), \sin(\alpha_{\mathbf{z}} + \alpha)\sin(\beta_{\mathbf{z}} + \beta), \cos(\alpha_{\mathbf{z}} + \alpha)\right]^T, \tag{2}$$

where $\alpha_{\mathbf{z}}$ and $\beta_{\mathbf{z}}$ are inclination and azimuth of $\mathbf{z}$, respectively. To rotate $\mathbf{z}$ to $\hat{\mathbf{z}}$, we define an additional rotation axis $\mathbf{z}^{\perp}$ and its rotation angle τ as follows:

$$\mathbf{z}^{\perp}(\alpha, \beta) = \frac{\mathbf{z} \times \hat{\mathbf{z}}(\alpha, \beta)}{\left\|\mathbf{z} \times \hat{\mathbf{z}}(\alpha, \beta)\right\|_2} \text{ and } \tau = \arccos\left(\mathbf{z}^T \cdot \hat{\mathbf{z}}(\alpha, \beta)\right). \tag{3}$$

Unfortunately, α and β are non-linear and vary with respect to a spherical coordinate system. To overcome this issue, we instead compute α and β as functions of unit-speed geodesics on the local tangent plane at $\mathbf{z}$ via the exponential map $\varphi_{\mathbf{z}}: T_{\mathbf{z}}\mathbb{S}^2 \to \mathbb{S}^2$. In this way, we can thus find a unique location $\mathbf{z}_T \in T_{\mathbf{z}}\mathbf{S}^2$ that corresponds to $\hat{\mathbf{z}}$. For two arbitrary orthonormal bases $\mathbf{u}_1, \mathbf{u}_2 \in T_{\mathbf{z}}\mathbb{S}^2$, α and β are determined by a linear combination of the two bases as follows:

$$[\alpha, \beta]^T = \varphi_{\mathbf{z}}(\mathbf{z}_T) = \varphi_{\mathbf{z}}\left(c_{\mathbf{u}_1}\mathbf{u}_1 + c_{\mathbf{u}_2}\mathbf{u}_2\right), \tag{4}$$

where $c_{\mathbf{u}_1}$ and $c_{\mathbf{u}_2}$ are coefficients associated with $\mathbf{u}_1$ and $\mathbf{u}_2$, respectively. Note that $\mathbf{u}_1$ and $\mathbf{u}_2$ define a reference frame on the tangent space, which has no influence on geodesics themselves on $T_{\mathbf{z}}\mathbb{S}^2$.

Rotation about Euler axis.—Given a rotation angle $\gamma \in [-\pi, \pi]$ about $\hat{\mathbf{z}}$, we compute the rigid rotation using the following Rodrigues rotation formula:

$$\mathbf{R}(\alpha,\beta,\gamma) = \left(\mathbf{I} + (\sin\gamma)[\hat{\mathbf{z}}]_\times + (1-\cos\gamma)[\hat{\mathbf{z}}]_\times^2\right) \cdot \left(\mathbf{I} + (\sin\tau)\left[\mathbf{z}^\perp\right]_\times + (1-\cos\tau)\left[\mathbf{z}^\perp\right]_\times^2\right), \tag{5}$$

where $[\hat{\mathbf{z}}]_\times$ and $[\mathbf{z}^\perp]_\times$ are the 3 × 3 skew symmetric matrices of $\hat{\mathbf{z}}$ and $\mathbf{z}^\perp$, which represent cross products, respectively. For $\forall \mathbf{x} \in \mathbb{S}^2$, this encodes a new location:

$$M(\mathbf{x}) = \hat{\mathbf{x}}(\alpha,\beta,\gamma) = \mathbf{R}(\alpha,\beta,\gamma)\cdot\mathbf{x}\,. \tag{6}$$

The resulting deformation M yields an identical rigid rotation at every location and globally drives the corresponding locations to the closest location by finding an optimal set of α, β, and γ, which needs an extension to non-rigid deformation.

2.3 Extension to Hierarchical Spherical Deformation

In general, all the corresponding locations are not completely aligned after the rigid rotation. This leads to an extension of the rigid rotation to non-rigid deformation. Here, we propose smoothly spatially-varying rotation angles (α, β, γ) as functions of spherical locations rather than constants. For this purpose, we use a spherical harmonics interpolation technique that allows smooth interpolation of signals defined on the unit sphere. At a spherical location (θ, ϕ), the spherical harmonics basis function of degree l and order m ($-l \le m \le l$) is given by

$$Y_l^m(\theta,\phi) = \sqrt{\frac{2l+1}{4\pi}\frac{(l-m)!}{(l+m)!}}P_l^m(\cos\theta)e^{im\phi}, \tag{7}$$

$$Y_l^{-m}(\theta,\phi) = (-1)^m Y_l^{m\,*}(\theta,\phi), \tag{8}$$

where $Y_l^{m\,*}$ denotes the complex conjugate of Y_l^m, and P_l^m is the associated Legendre polynomial

$$P_l^m(x) = \frac{(-1)^m}{2^l l!}\left(1-x^2\right)^{\frac{m}{2}}\frac{d^{(l+m)}}{dx^{(l+m)}}\left(x^2-1\right)^l. \tag{9}$$

In particular, α and β are obtained by plugging a set of spherical harmonics coefficients $\mathbf{c}_{\mathbf{u}_1} = \left\{c_{l,\mathbf{u}_1}^m\right\}$ and $\mathbf{c}_{\mathbf{u}_2} = \left\{c_{l,\mathbf{u}_2}^m\right\}$ into Eq. (4):

$$[\alpha(\theta,\phi),\beta(\theta,\phi)]^T = \varphi_{\mathbf{z}}\left(\sum_{l=0}^{\infty}\sum_{m=-l}^{l}\left(c_{l,\mathbf{u}_1}^m\mathbf{u}_1 + c_{l,\mathbf{u}_2}^m\mathbf{u}_2\right)\cdot Y_l^m(\theta,\phi)\right). \tag{10}$$

This locally defines $\hat{\mathbf{z}}$. Similarly, γ is obtained by the spherical harmonics interpolation as a function of spherical harmonics coefficients $\mathbf{c}_\gamma = \left\{c_{l,\gamma}^m\right\}$.

$$\gamma(\theta,\phi)=\sum_{l=0}^{\infty}\sum_{m=-l}^{l}c_{l,\gamma}^{m}\cdot Y_{l}^{m}(\theta,\phi)\,. \tag{11}$$

This locally defines a rotation about $\hat{\mathbf{z}}$ at each spherical location (θ, ϕ), which implies that the rotation smoothly changes across spherical locations. The proposed deformation is hierarchically represented since the spherical harmonics basis functions are linearly independent; the lower spherical harmonics degree, the smoother, more global deformation. Thus, the smoothness is easily controllable. Note that the deformation is equivalent to a rigid (global) rotation if $l=0$.

2.4 Optimization

We use scalar maps (e.g., mean curvature) defined on the cortical surfaces for the registration metric. We evaluate the agreement of the deformed scalar maps on the unit sphere to find the optimal Euler angles. Since an explicit correspondence of scalar maps is unavailable, we instead put S icosahedral sampling points on each subject's sphere and evaluate the agreement of the deformed scalar maps at the corresponding sampling locations. Given estimates of $\mathbf{c}_{\mathbf{u}_1}^{i}$, $\mathbf{c}_{\mathbf{u}_2}^{i}$, $\mathbf{c}_{\gamma}^{i}$ of the ith subject, we consider its scalar map m^i and the corresponding location $\mathbf{x}_j^i$ to the jth sampling location $\mathbf{x}_j$ such that $\mathbf{x}_j=\mathbf{R}\left(\mathbf{c}_{\mathbf{u}_1}^{i},\mathbf{c}_{\mathbf{u}_2}^{i},\mathbf{c}_{\gamma}^{i}\right)\cdot\mathbf{x}_j^i$ (see Eq. (6)). By letting $\bar{m}_j$ be the mean across scalar maps at $\mathbf{x}_j$, the energy function is given by

$$E\left(\mathbf{c}_{\mathbf{u}_1},\mathbf{c}_{\mathbf{u}_2},\mathbf{c}_{\gamma}\right)=\frac{1}{2SN}\sum_{j=1}^{S}\sum_{i=1}^{N}\frac{1}{\sigma_{\mathbf{x}_j}^{2}}\cdot\left(m^{i}\left(\mathbf{x}_j^{i};\mathbf{c}_{\mathbf{u}_1}^{i},\mathbf{c}_{\mathbf{u}_2}^{i},\mathbf{c}_{\gamma}^{i}\right)-\bar{m}_j\right)^{2}, \tag{12}$$

where $\sigma_{\mathbf{x}_j}^{2}$ is feature variance at $\mathbf{x}_j$. By assuming that $\bar{m}$ and $\sigma_{\mathbf{x}}^{2}$ are constant, we have the following gradients by some algebra:

$$\begin{aligned}-\frac{\partial E}{\partial c_{l,\mathbf{u}}^{m}}=&\frac{1}{SN}\sum_{j=1}^{S}\sum_{i=1}^{N}\frac{1}{\sigma_{\mathbf{x}_j}^{2}}\cdot Y_{l}^{m}\left(\theta_{\mathbf{x}_j^i},\phi_{\mathbf{x}_j^i}\right)\cdot\left([\mathbf{z}\times\mathbf{u}]_{\times}\cdot\mathbf{x}_j\right)^{T}\cdot\nabla_{\mathbf{x}_j}m^{i}\\&\cdot\left(\bar{m}_j-m^{i}\left(\mathbf{x}_j^{i}\right)\right),\end{aligned} \tag{13}$$

$$-\frac{\partial E}{\partial c_{l,\gamma}^{m}}=\frac{1}{SN}\sum_{j=1}^{S}\sum_{i=1}^{N}\frac{1}{\sigma_{\mathbf{x}_j}^{2}}\cdot Y_{l}^{m}\left(\theta_{\mathbf{x}_j^i},\phi_{\mathbf{x}_j^i}\right)\cdot\left([\hat{\mathbf{z}}]_{\times}\cdot\mathbf{x}_j\right)^{T}\cdot\nabla_{\mathbf{x}_j}m^{i}\cdot\left(\bar{m}_j-m^{i}\left(\mathbf{x}_j^{i}\right)\right), \tag{14}$$

where $\nabla_{\mathbf{x}}m$ is a spatial gradient that can be efficiently computed as proposed in [7]. The optimal coefficients are then obtained by a standard gradient descent technique. Due to the nonlinearity of the energy function, the optimization is first preformed incrementally on each individual degree from $l=0$ for an initial guess [4]. We also estimate $\bar{m}$ and $\sigma_{\mathbf{x}}^{2}$ from

initial scalar maps and then update them during the initial guess to employ improved population statistics. Finally, the spherical harmonics coefficients are tuned simultaneously, which drives all the deformation fields with rigid and non-rigid deformation at the same time.

3 Results

We randomly chose 14 subjects out of the OASIS dataset [5]. Each hemisphere was manually labeled by an expert via the brainCOLOR protocol (49 ROIs)[1]. The evaluation was based on the surface parcellation and registration distortion. The cortical surfaces were reconstructed via a standard FreeSurfer pipeline [2], and the left hemispheres were used. We compared the proposed method with two existing methods with their default parameter settings: FreeSurfer (fixed template) [3] and Spherical Demons (fixed population average) [7]. In our method, we empirically set $l = 10$. All experiments were conducted with a single thread (Intel Xeon E5–2630 2.20GHz). For each subject, the proposed method and Spherical Demons took less than 3 mins, whereas FreeSurfer took more than an hour.

3.1 Registration Metrics

First, we computed the registration results using convexity (*sulc*) and rough/fine curvature (*curv*) features of the FreeSurfer's outputs that are optimized for FreeSurfer and Spherical Demons. In these methods, the registration was achieved in a multi-scale manner by aligning *sulc* and rough *curv* maps followed by fine *curv* maps. Similarly, we varied the number of the sampling points at four different levels of icosahedral subdivision from 4 ($S = 2, 562$) to 7 ($S = 163, 842$). Unlike [7], we performed only a single round of co-registration, which yields much faster registration. Second, we evaluated the three methods for their flexibility of deformation with only a fine *curv* feature having many local homogeneous regions. Here, we used $S = 163, 842$. Figure 2 shows the average fine *curv* features. Overall, similar patterns were observed in the three methods with all features since rough features provided well initial alignments in the low scales. On the other hand, the use of a fine *curv* feature yielded a less alignment in FreeSurfer and Spherical Demons, whereas the proposed method offered a comparable alignment to that with all features. Our method also produced less biased average population patterns than FreeSurfer that refers to a specific template.

3.2 Cortical Surface Parcellation

Since no ground-truth parcellation was available, we computed the mode parcellation map across the subjects. Then, we computed a Dice coefficient for each region with the mode map. We performed one-sided t-tests to reveal regions with statistically significant improvement on Dice coefficients. In addition, we corrected p-values via multi-comparisons using a standard false discovery rate [1] at $q = 0.05$. Table 1 and Table 2 summarize the Dice coefficients and the revealed regions, respectively. One improved region was found with all features compared to FreeSurfer, while showing comparable results to Spherical Demons. The proposed method achieved a high Dice coefficient even with only a fine *curv* feature; a large number of regions were revealed with significant improvement because the ambiguity

[1]Neuromorphometrics, Inc. http://www.neuromorphometrics.com/

in the local homogeneity of the highly localized feature maps was reduced by harmonizing rigid and non-rigid deformation.

3.3 Registration Distortion

Again, measuring registration distortion is important to evaluate bias introduced by deformation fields, which could affect secondary statistical shape analyses. We measured area and length distortion for each triangle and edge as the absolute log ratio between before and after registration [6]. Table 3 summarizes registration distortion in the three methods. Our method provided significantly reduced registration distortion compared to FreeSurfer and Spherical Demons regardless of registration metrics. We emphasize that such reduced distortion is achieved while keeping comparable registration accuracy to the existing methods.

4 Conclusion

We presented novel spherical deformation for a shape correspondence. The proposed method extends the rigid rotation represented by Euler angles to general non-rigid deformation. Both rigid rotation and non-rigid deformation are updated simultaneously in a single framework. Moreover, the proposed method is group-wise registration that does not require a specific template. Consequently, the resulting deformation field is smooth, continuous, and independent of a particular spherical coordinate system. In the experiments, the proposed method showed high accuracy in cortical surface parcellation as well as low registration distortion compared to the existing methods.

Acknowledgments.

This work was supported in part by the National Institutes of Health (NIH) under Grant R01EB017230, Grant R01MH102266, Grant R01MH091645, Grant R01MH098098, Grant P30HD003110, and Grant U54HD079124, and in part by the VISE/VICTR under Grant VR3029.

References

1. Benjamini Y, Hochberg Y: Controlling the false discovery rate: a practical and powerful approach to multiple testing. Journal of the royal statistical society. Series B (Methodological) pp. 289–300 (1995)
2. Dale AM, Fischl B, Sereno MI: Cortical surface-based analysis: I. segmentation and surface reconstruction. Neuroimage 9(2), 179–194 (1999) [PubMed: 9931268]
3. Fischl B, Sereno M, Tootell R, Dale A: High-resolution intersubject averaging and a coordinate system for the cortical surface. Human Brain Mapping 8(4), 272–284 (1999) [PubMed: 10619420]
4. Lyu I, Kim SH, Seong JK, Yoo SW, Evans A, Shi Y, Sanchez M, Niethammer M, Styner MA: Robust estimation of group-wise cortical correspondence with an application to macaque and human neuroimaging studies. Frontiers in Neuroscience 9, 210 (2015) [PubMed: 26113807]
5. Marcus DS, Wang TH, Parker J, Csernansky JG, Morris JC, Buckner RL: Open access series of imaging studies (oasis): cross-sectional mri data in young, middle aged, nondemented, and demented older adults. Journal of cognitive neuroscience 19(9), 1498–1507 (2007) [PubMed: 17714011]
6. Robinson EC, Garcia K, Glasser MF, Chen Z, Coalson TS, Makropoulos A, Bozek J, Wright R, Schuh A, Webster M, et al.: Multimodal surface matching with higher-order smoothness constraints. NeuroImage 167, 453–465 (2018) [PubMed: 29100940]

7. Yeo B, Sabuncu M, Vercauteren T, Ayache N, Fischl B, Golland P: Spherical demons: Fast diffeomorphic landmark-free surface registration. IEEE Transactions on Medical Imaging 29(3), 650–668 (2010) [PubMed: 19709963]

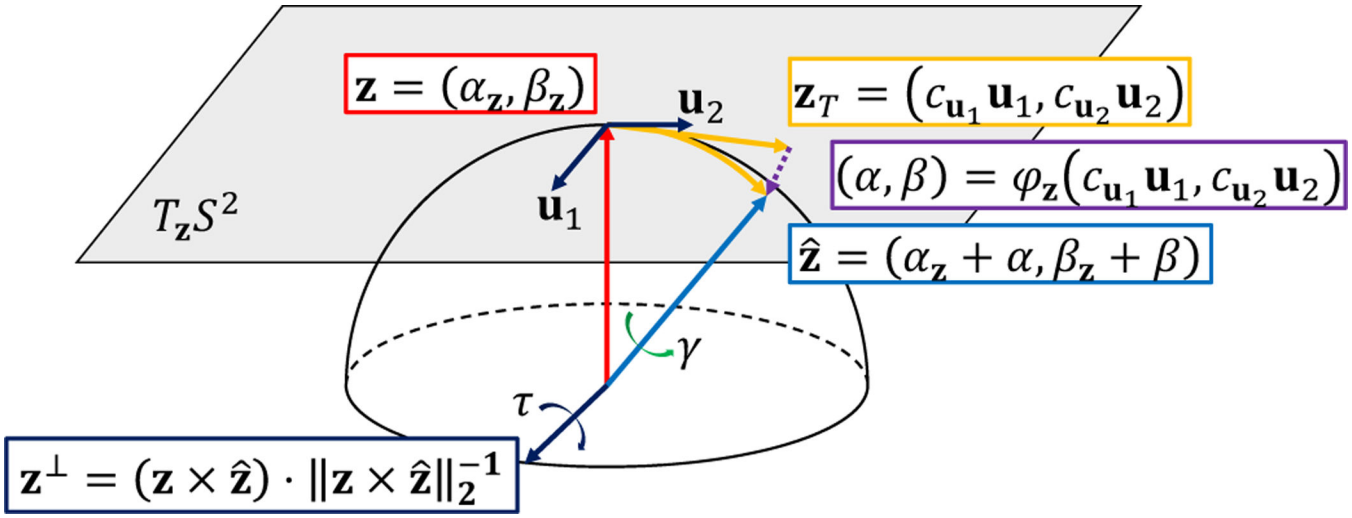

Fig.1.

A schematic illustration of the proposed rotation by Euler angles α, β, and γ. For the rotation of a given location, the rotation axis $\mathbf{z}$ (*red*) is rotated to $\hat{\mathbf{z}}$ (*blue*) by α and β (i.e., τ about $\mathbf{z}^{\perp}$), followed by a rotation about $\hat{\mathbf{z}}$ by γ (*green*). Since α and β are inconsistent subject to the poles of a spherical coordinate system, the exponential map φ (*violet*) at $\mathbf{z}$ is employed to encode local geodesics (*orange*). Overall, the rotation axis $\hat{\mathbf{z}}$ and its associated rotation angle γ smoothly vary on the unit sphere as functions of spherical locations. A half sphere is used for better visualization.

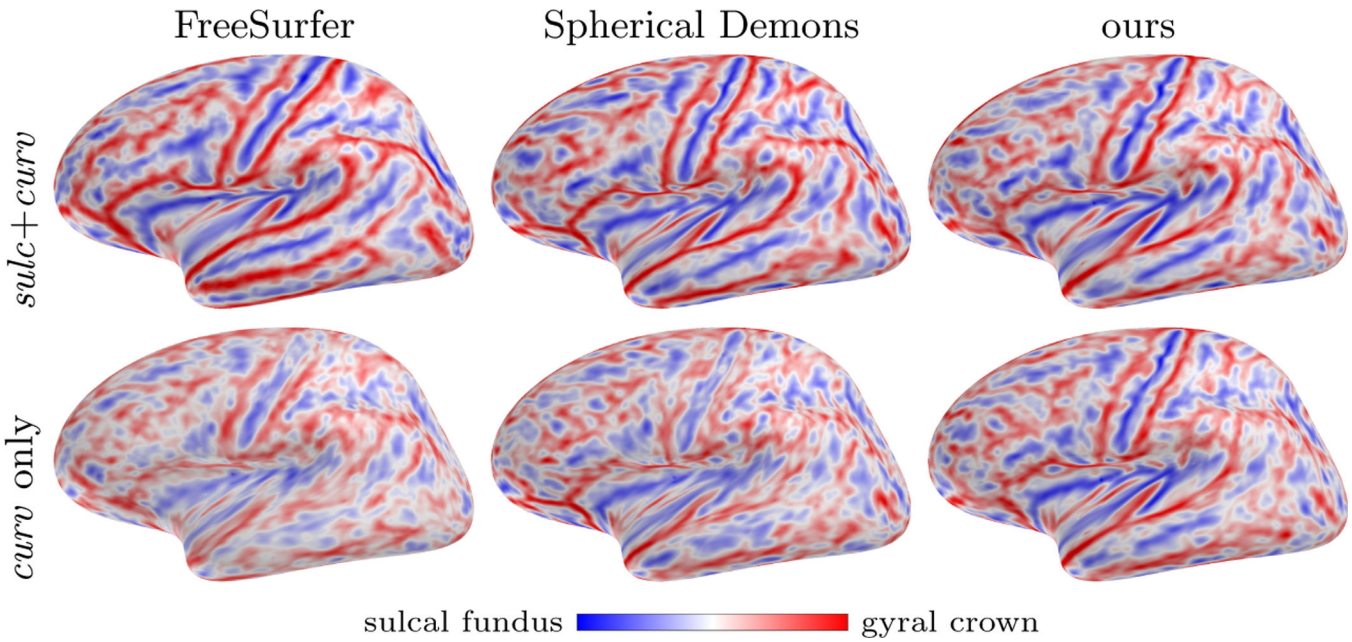

Fig.2.

The average fine *curv* feature maps. The three methods achieve similar *curv* patterns with *sulc*+*curv*. On the other hand, FreeSurfer and Spherical Demons show less aligned *curv* maps with only a fine *curv* feature due to the local homogeneity, whereas the proposed method provides a comparable result to that with *sulc*+*curv*.

Table 1.

Overall Dice coefficient in cortical surface parcellation. Compared to FreeSurfer and Spherical Demons, the proposed method achieves comparable Dice coefficients with *sulc*+*curv* and better overlaps with *curv* (*$p \ll$ 001). See Table 2 for more details about individual regions with significantly improved Dice coefficients.

metric	FreeSurfer	Spherical Demons	ours
sulc+*curv*	0.782 ± 0.132	0.784 ± 0.133	0.785 ± 0.129
curv only	0.692 ± 0.164	0.728 ± 0.155	0.774 ± 0.130*

Table 2.

The number of regions with statistical significance (# of increases/# of decreases). One-sided *t*-tests reveal regions with statistical significance after multi-comparison correction ($q = 0.05$). No region is found with a decreased Dice coefficient.

metric	FreeSurfer	Spherical Demons
sulc+*curv*	1/0	0/0
curv only	40/0	23/0

Table 3.

Registration distortion: absolute log ratio (mean ± std (max)) in surface area and edge length. For both *sulc* +*curv* and *curv* features, the proposed method yields significantly less registration distortion than FreeSurfer and Spherical Demons by showing statistical significance (*$p \ll 001$).

	metric	FreeSurfer	Spherical Demons	ours
area	*sulc*+*curv*	0.268 ± 0.217 (8.045)	0.194 ± 0.166 (2.986)	0.164 ± 0.130 (1.050)*
	curv only	0.243 ± 0.214 (10.722)	0.113 ± 0.101 (3.007)	0.090 ± 0.075 (0.662)*
len	*sulc*+*curv*	0.178 ± 0.150 (4.330)	0.129 ± 0.108 (1.980)	0.102 ± 0.083 (0.747)*
	curv only	0.156 ± 0.138 (5.398)	0.072 ± 0.066 (1.316)	0.055 ± 0.046 (0.438)*